Electrical breakdown at semiconductor grain boundaries

G. Blatter and F. Greuter
Brown Boveri Research Center, CH-5405 Baden-Dättwil, Switzerland
(Received 16 May 1986)

Carrier transport through electrically active grain boundaries is studied under high-electric-field conditions. Electrons trapped at the interface and screened by ionized shallow and deep bulk defects are responsible for the formation of double Schottky barriers which reduce the carrier flow by several orders of magnitude. At large applied bias, electric fields up to 1 MV/cm can build up near the interface, leading to the generation of hot electrons and to the subsequent production of holes by impact ionization. This process is studied in a realistic model, taking the inhomogeneous field as well as longitudinal-optic and -acoustic phonon scattering into account. The hot-electron distribution function is calculated as the solution of a Fokker-Planck equation in energy space. With a reasonable estimate for the pair-creation rate we determine the yield for hole production near the interface. These minority carriers are swept back to the grain boundary where they serve as an additional screening charge for the electrons. We determine the steady-state and dynamic behavior of the barrier, including the holes in our calculations. The accumulation of holes at the interface can lead to the breakdown of the barrier which, in its most dramatic form, can even result in a bistability. The dynamic behavior of the barrier reflects the presence of holes through the development of a negative capacitance, in agreement with experimental observations. The negative capacitance is explained by the finite recombination time of the holes at the interface. In a model where the recombination is substituted by hole emission, a realistic current-voltage characteristic but no negative capacitance is found.

I. INTRODUCTION

The physics of grain boundaries in semiconductors is of interest both from a fundamental as well as from a technical point of view.[1] In recent years the understanding of many basic problems as, e.g., the atomic and electronic structure[2,3] of such interfaces has increased significantly. The growing number of technical applications which take advantage of polycrystalline materials (electronic devices and solar cells based on poly-Si, ZnO varistors, boundary-layer capacitors) asks for a more thorough knowledge of the underlying structural and electronic phenomena.

Carrier transport through grain boundaries, in particular, is a vital aspect of the physics of grain boundaries, as the electrical properties of the polycrystalline material can be vastly different from those of the constituent crystalline bulk. Therefore the electrical properties of grain boundaries have been extensively studied experimentally as well as theoretically.[1,4–14] Measurements of the static I-V characteristics, the dynamical response [deep-level transient spectroscopy (DLTS), admittance], and optical spectroscopy have been used to gain information on the microscopic parameters of grain boundaries as, e.g., density, energy position, and trapping cross sections of interface states and defect states in the adjacent bulk material. Models describing the electrical properties of grain boundaries have been developed by Seager and Pike[7,12] and by Werner[11] and a complete description, including the effects of deep bulk trap states, has been presented recently by Blatter and Greuter[14] (hereinafter denoted as BG).

The electrical behavior of grain boundaries is governed by double Schottky barriers resulting from electrons trapped at the interface and screened by ionized shallow and deep bulk defects. In BG it has been shown that the interface density of states, the shallow bulk defects, as well as the existence of deep volume traps, have a strong influence on the static and dynamic properties of the carrier transport. In particular, the additional screening charge provided by the deep bulk defects tends to destabilize the barrier, and the finite response time for their charge transfer contributes to the small-signal behavior of the junction.

In the present paper we generalize the model by including the new phenomena observed in the high-field regime. In this electrical breakdown region, the generation of minority carriers by hot electrons has to be included. The importance of these effects has been proposed by Pike.[15] At large applied bias V, electric fields up to 1 MV/cm can build up near the interface, leading to the generation of hot electrons and the subsequent production of holes by impact ionization of valence states. Holes diffusing back to the interface compensate part of the trapped negative charge and thereby lower the potential barrier. This results in a steep increase of the current density j and in a large nonlinearity coefficient $\alpha = d(\ln j)/d(\ln V)$ as observed in the experiments. The finite recombination time of the holes at the interface produces an additional dynamic capacitance with an opposite sign. Thereby it is possible to explain, within the framework of this model, the experimentally observed overall negative capacitance at breakdown. Direct confirmation for the presence of minority carriers at grain boundaries is given by the observation of band-gap electroluminescence in GaAs (Ref. 16) and ZnO (Ref. 17).

In the original paper by Pike,[15] the breakdown mechanism is discussed under simplified assumptions in order to illustrate the correctness of the model. It is the aim of the present paper to give a detailed and complete description of the carrier transport through grain boundaries including deep bulk traps and minority carrier effects. This includes (i) a realistic description of the distribution function for hot electrons in large inhomogeneous fields, (ii) the calculation of the hole production as a function of applied bias, and (iii) a self-consistent description of the static and dynamic properties of the carrier transport. We will show that, depending on the details of the model, very different behavior of transport can be found: In the case where all holes diffusing back are trapped at the interface, the barrier becomes unstable as a result of the *barrier-controlled avalanche breakdown.* This leads to a negative differential resistance (or bistability) in the current-voltage characteristic—the most extreme case of a nonlinearity with a divergent α at breakdown bias.

A stabilization of the barrier is obtained by the introduction of a finite density of hole traps at the interface, such that only a fraction of the minority carriers diffusing back are trapped. For the case where *hole recombination* is the dominant process in determining the density of holes at the interface, we can find a stable breakdown, high α values, and a negative small-signal capacitance. For the situation where *hole emission* is the dominant process (no recombination) we again find a stable barrier breakdown but no negative capacitance. This shows that the pair recombination process at the interface is crucial to the understanding of the negative capacitance observed at large bias.

The paper is organized as follows. In Sec. II we discuss the main ideas and the results of a calculation for the pair creation in the high electric fields near the grain boundaries. Details of this calculation will be published in a separate paper, as the method can be applied to a variety of similar problems. In Sec. III we use the results of Sec. II for the description of the steady-state properties of the interfacial potential barrier. The time-dependent properties of the carrier transport are discussed in Sec. IV and the main results are summarized in Sec. V. For simplicity we use a single-level density of interface states to illustrate the calculation. The general case of a continuous density is discussed in the Appendix, where two models of interface relaxation (strongly localized traps or perfect relaxation among the interface levels) are handled as in our previous paper.[14]

For the numerical results we use material parameters appropriate to ZnO, as doped polycrystalline ZnO probably represents the most thoroughly studied system concerning these breakdown effects. However in the present paper no effort is made to fit a particular type of ZnO varistor. The direct comparison of the theoretical considerations (including BG) to the actual experimental data will then be given in the final paper of this series.

II. HOT ELECTRONS AND PAIR CREATION

As a result of broken translational symmetry, deep-lying energy states may be formed at the boundaries of semiconductor grains. These states may be viewed as dangling bounds or other interfacial defect states like, e.g., levels derived from impurity atoms trapped at the interface. The width of such an interfacial region typically amounts to approximately 10 Å (Refs. 2 and 18) and therefore the idealization as an infinitely thin charged interface, with trapping levels of acceptor or donor type, is well justified. We restrict the discussion to a negatively charged interface in an n-type semiconductor.

The potential felt by the charge carriers near the plane interface is easily calculated in the Schottky approximation (energy-band diagram, see Fig. 1). Assuming for simplicity only one homogeneously distributed, shallow bulk defect with density N_0, we have to solve the Poisson equation

$$\frac{d^2}{dx^2}\Phi(x)=\frac{\rho(x)}{\epsilon_0\epsilon}$$

for the potential $\Phi(x)$, given the charge distribution $\rho(x)$,

$$\rho(x)=eN_0[\Theta(x+x_{l0})-\Theta(x-x_{r0})]-Q_i\delta(x)\ .$$

Here Q_i denotes the interface charge, ϵ is the static dielectric constant, ϵ_0 the permittivity of the vacuum, and e the unit charge [$e=|e|$, $e\Phi(x)$=potential energy of the electron]. The boundaries of the screening charge are denoted by $-x_{l0}$ and x_{r0}, and $\Theta(x)$, $\delta(x)$ denote the Heaviside unit step function and the Dirac δ function, respectively. Using the boundary conditions

$$\Phi(-\infty)=\Phi(-x_{l0})=0 \text{ and } \Phi(\infty)=\Phi(x_{r0})=-V\ ,$$

the condition for continuity at $x=0$, as well as charge neutrality,

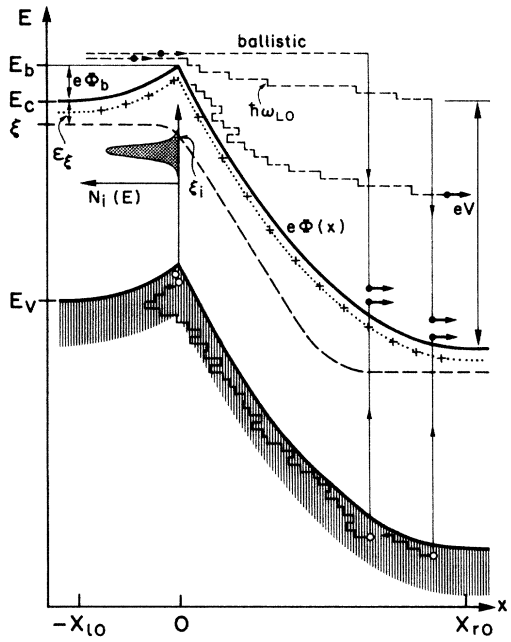

FIG. 1. Energy-band diagram for a double Schottky barrier at a grain boundary under large applied bias V. The mechanisms of hot-electron transport and pair creation are sketched.

$$\Phi(0^-)=\Phi(0^+)=\Phi_b,\quad \Phi'(0^-)-\Phi'(0^+)=Q_i/\epsilon_0\epsilon\ ,$$

the solution is found immediately:

$$\Phi(x)=\begin{cases}\dfrac{\gamma_0}{2}(x+x_{l0})^2, & -x_{l0}\le x\le 0\ ,\\ \dfrac{\gamma_0}{2}(x-x_{r0})^2-V, & 0\le x\le x_{r0}\ ,\end{cases}$$

with $\gamma_0=eN_0/\epsilon_0\epsilon$ and the boundaries

$$x_{l0}=\left[\frac{V_c}{2\gamma_0}\right]^{1/2}\left[1-\frac{V}{V_c}\right],\quad x_{r0}=\left[\frac{V_c}{2\gamma_0}\right]^{1/2}\left[1+\frac{V}{V_c}\right],$$

$$V_c=\frac{1}{2\gamma_0}\left[\frac{Q_i}{\epsilon_0\epsilon}\right]^2 .$$

The barrier height Φ_b depends on the interface charge Q_i and on the applied bias V,

$$\Phi_b=\tfrac{1}{4}V_c\left[1-\frac{V}{V_c}\right]^2, \tag{1}$$

and disappears smoothly as $V\to V_c$. The remaining free parameter, the interface charge $Q_i(V)$, is determined by the interface density of states (DOS) $N_i(E)$. Q_i has to be determined self-consistently, as $N_i(E)$ is fixed with respect to the valence band at $x=0$:

$$Q_i[\Phi_b(V)]=e\int_{\xi_i^n} dE\, N_i(E)f_i(E)\ , \tag{2}$$

with

$$f_i(E)=\frac{1}{1+e^{(E-\xi_i)/k_BT}}\ .$$

Here ξ_i is the quasi-Fermi-level at the interface which deviates from the bulk Fermi level ξ for $V>0$,[19(a),(b)]

$$\Delta\xi=\xi-\xi_i=k_BT\ln\left[\frac{2}{1+e^{-eV/k_BT}}\right].$$

The shift $\Delta\xi$ is determined by the detailed balance condition for charge trapping and emission by the interface. ξ_i^n is the Fermi level of the neutral interface.[6]

The behavior of the barrier Φ_b as a function of applied bias V for different forms of the DOS $N_i(E)$, and for the general case including additional screening by deep bulk states, is thoroughly discussed in BG. Here we focus on the new phenomena introduced by the generation of hot electrons at large applied bias and the production of holes by impact ionization.

The main part of this section is organized in the following way. After a short review of the phenomena involved, we discuss the different scattering mechanisms which we have considered to be the most important in this problem: longitudinal optical phonons, acoustic phonons, impurity scattering, and electron-hole pair creation. We then determine the distribution function for the hot electrons with the help of a Fokker-Planck equation in energy space. Finally the total amount of pairs created in the depletion region is calculated.

In a first step we consider the transport of the electrons injected thermally over the barrier into the positively biased grain. For the case of a pure ballistic transport, all the potential energy of the electron is converted into kinetic energy E_k (see Fig. 1).

As E_k overcomes a threshold energy $E_{\rm th}$, the electron can impact ionize a valence state and thereby create a hole. The threshold $E_{\rm th}$ is determined by conservation of energy and momentum during pair creation, and a straight-forward calculation with parabolic valence and conduction band yields

$$E_{\rm th}=\frac{m_v+2m_c}{m_v+m_c}E_g\ .$$

Here m_v and m_c are the effective masses of the valence (heavy hole) and the conduction band, respectively, and E_g is the (direct) energy gap.

Since the depletion region, in which the electron is accelerated, typically extends over approximately 10^3 Å the transport is not ballistic in general: assume an electron is travelling through the depletion region starting at the interface at $x=0$. The amount of kinetic energy picked up by the electron is equal to the potential-energy difference between $x=0$ and its momentary position x. This energy does not depend on the path of the carrier since the field is stationary and conservative. The trajectory of the electron depends on the scattering events suffered in the depletion region. Elastic events do not cost energy, however, they have the tendency to lengthen the trajectory of the electron. This enhances the probability to undergo an inelastic event, which costs energy, and thereby the kinetic energy of the particle arriving at x is reduced. (Note that this situation is somewhat different from the one encountered in avalanche breakdown in insulators by laser radiation, where the electric field is time dependent.[20]) We then have to study two types of events: (i) elastic scattering which changes the particles trajectory, and (ii) inelastic scattering which costs energy besides changing the path of the carrier.

At this stage we have to restrict the discussion to a certain type of material. Here we treat the case of ZnO which is a very polar material. Therefore scattering by *longitudinal optical* (LO) phonons *(Fröhlich scattering*[21]*)* is the dominant energy loss process. ZnO has wurtzite structure with only one LO phonon (energy $\hbar\omega_{\rm LO}=72$ meV) which generates a macroscopic polarization field and therefore couples to the electrons.[22] The dimensionless coupling constant α (Ref. 23)

$$\alpha=\frac{1}{4\pi\epsilon_0}\frac{e^2}{\hbar}\left[\frac{m_c}{2\hbar\omega_{\rm LO}}\right]^{1/2}\left[\frac{1}{\epsilon_\infty}-\frac{1}{\epsilon}\right]\cong 1.1$$

(ϵ_∞ is the high-frequency dielectric constant) is of intermediate strength and the rate of phonon emission typically is approximately $10^{14}\ {\rm s}^{-1}$. (We can neglect corrections by stimulated emission and by absorption for the temperatures considered here, $T\lesssim 400$ K.) The calculated LO-phonon contribution to the scattering rates (per unit time: Γ, per unit length: $1/\lambda$) as a function of kinetic energy E_k is shown in Fig. 2. Fröhlich scattering is most effective at low electron energies ($E_k\lesssim 0.5$ eV) and decreases

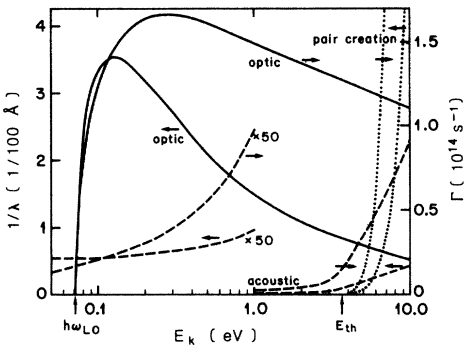

FIG. 2. Scattering rates per unit length ($1/\lambda$) and per unit time (Γ) as a function of the kinetic energy E_k of the electrons. The rates for optic and acoustic scattering and for pair creation, are shown.

slowly for increasing energy. The scattering geometry also depends strongly on energy: For low energies the momentum of the scattered particle is distributed isotropically, with respect to the incident momentum, whereas the scattering becomes forward directed at higher energies.

Next we consider scattering by *longitudinal acoustic* phonons. For low electron energies we can calculate the deformation potential scattering once we know the effective coupling constant. Here the literature[24] presents values ranging from 3.6 to 18.9 eV. We have performed a very simple microscopic calculation for the momentum-(q)-dependent scattering potential, based on the ionic screening from the nearest neighbors. For $q \to 0$ we find a deformation potential of approximately 5 eV which is reasonable. Unlike the behavior for LO phonons, the acoustic scattering rate is low at small energies ($E_k \lesssim 5$ eV) but increases strongly and is dominant at high energies (see Fig. 2). Note that with increasing energy E_k, phonons with large momenta ($k > k_{BZ}/2$, k_{BZ} is the wave number at the Brillouin zone) and finite energies (approximately 50 meV) play the major role (large phase space). Despite the low rate, compared to the LO phonons, the acoustic phonons are very efficient scatterers because of the large momentum transfer involved (umklapp scattering). The geometry of the scattering can be reasonably approximated by an isotropic ansatz for the scattering angles. High-energy electrons moving along the field direction are therefore deflected away and suffer a considerable path lengthening. Hence these electrons are efficiently cooled on their way through the depletion region.

As the energy of the electron increases even further ($E_k > 25$ eV), the scattering becomes forward directed again, but these energies are beyond the region of interest for the present problem.

Let us now turn to *impurity scattering*. The rate of this Rutherford-type scattering is immediately calculated.[25] Since there is a lack of free-electron screening charge for the ionized donors in the depletion region, we use the concept introduced by Conwell and Weisskopf[26] for the determination of the long-wavelength cutoff: no scattering momenta $q < 4\pi N_0^{1/3}$ are taken into account, as these long wavelengths correspond to the smooth space variation of the electrostatic potential incorporated already in $\Phi(x)$. For the present situation ($N_0 \sim 10^{18}$ cm^{-3}) the scattering rate is of the order of $10^{14}\,[E_k/(1\text{ eV})]^{1/2}$ s^{-1} which is quite large at energies in the eV range. However, the following two properties keep the role of impurity scattering in electron cooling small compared to the other processes: Impurity (Rutherford) scattering is (i) elastic and (ii) highly forward directed for energies above approximately 0.1 eV. Taking into account the energy dependence of the rate ($\Gamma \to 0$ as $E_k \to 0$), we find that the electrons are accelerated without scattering to energies where they are predominantly forward scattered by the impurities.

Finally let us consider the process of electron-hole *pair creation*. The correct expression for the rate, given by Fermi's "gold rule," amounts to the calculation of a twelvefold integral.[27,28] We circumvent this laborious task by resorting to Kane's random-k approximation,[27] which has been proven to be very accurate and useful in practical applications.[28,29] Within this approximation, the rate is not determined by energy and momentum conservation but rather by the phase-space volume open for the process. The pair-creation rate then has the energy dependence $\Gamma \sim (E_k - E_g)^{7/2}\Theta(E_k - E_{\text{th}})$, with a prefactor depending on the densities of states of the conduction and valence bands involved, as well as on the matrix element for the transition. This matrix element is very difficult to calculate and therefore we use Kane's data for silicon as a first estimate.[27] A plot of the pair-creation rate obtained within these approximations is given in Fig. 2.

As to other scattering processes, we have not taken into account (free-electron-like) plasma oscillations, as their energies are much too high (approximately 19 eV). Neither did we consider low-energy (approximately 40 meV) plasmons due to the finite carrier density in the conduction band, as these carriers are repelled from the depletion regions. By the same reasoning we also can neglect electron-electron scattering.

After the study of the scattering processes, we turn to the transport properties of the electrons in large electric fields.[30–35] Many models for the calculation of ionization rates as a function of applied field have been published in the past.[36–41] Most of these studies however apply to nonpolar semiconductors as Si or Ge, where scattering is treated isotropically. Dumke[42] has calculated the distribution function and the ionization rates for hot electrons in polar semiconductors (InSb and InAs) under homogeneous field conditions, including the polar forward scattering. Here we have studied the general case of *inhomogeneous fields* and have also taken the energy dependence of the scattering rates and the scattering geometry into account. Following the ideas of Uhlenbeck and Ornstein[43] we describe the distribution function $j(E_k,x)$ (spectral current density) by a *Fokker-Planck* equation in energy space,

$$\frac{\partial}{\partial x} j(E_k,x) = -\frac{\partial}{\partial E_k}\left[\frac{\langle \Delta E_k \rangle}{\Delta x} j(E_k,x)\right] + \frac{1}{2}\frac{\partial^2}{\partial E_k^2}\left[\frac{\langle (\Delta E_k)^2 \rangle}{\Delta x} j(E_k,x)\right]. \quad (3)$$

At the interface $x=0$ the thermal distribution of injected electrons represents the starting (initial) condition. The boundary conditions for $x>0$ are the following: (i) tunnelling current entering at $E_k=0$ and (ii) free boundaries for $E_k\to\infty$. The two coefficients $\langle\Delta E_k\rangle/\Delta x$ and $\langle(\Delta E_k)^2\rangle/\Delta x$ describe *drift* and *diffusion* in energy space, respectively. They depend on both position x (electric field) and energy. We have performed a path-integral-like calculation for these two quantities, taking LO-phonon scattering into account. Here we just give a heuristic argument for the calculation of the dominant drift term and postpone the details to a forthcoming publication.

The drift $\langle\Delta E_k\rangle/\Delta x$ consists of a gain in energy by the electric field, $e\mathscr{E}(x)=-e\,\Delta\Phi/\Delta x$, and a loss due to LO-phonon scattering, $\hbar\omega_{\rm LO}\langle\Delta n\rangle/\Delta x$. Here $\langle\Delta n\rangle$ is the average number of LO phonons emitted by the electron over a small distance Δx. For an estimate of $\langle\Delta n\rangle/\Delta x$ we calculate the distance Δx which the particle travels, emitting exactly Δn phonons on its way:

$$\Delta x=\sum_{i=1}^{\Delta n} v_i z_i t_i+\tfrac{1}{2}\sum_{i=1}^{\Delta n}\frac{e\mathscr{E}(x_i)}{m_c}t_i^2 .$$

Here $z_i=\cos\theta_i$, where θ_i is the angle of the momentum of the particle after the phonon emission, taken with respect to the field direction. For Δx small enough the velocities v_i and the field values $\mathscr{E}(x_i)$ can be taken as constant. Performing the (independent) averages over angles and scattering times t_i we find

$$\langle\Delta x\rangle=\lambda\left[\langle z\rangle+\frac{e\mathscr{E}(x)\lambda}{2E_k}\right]\Delta n ,$$

with the *mean free path* $\lambda=v/\Gamma$. Instead of averaging Δx for a given Δn, we should calculate the average $\langle\Delta n\rangle$ for a given distance Δx. The result of the path-integral calculation, which does this average properly, agrees within a few tenths of a percent with the above result and we therefore write

$$\frac{\langle\Delta n\rangle}{\Delta x}=\frac{1}{\lambda}\frac{1}{\langle z\rangle+\dfrac{e\mathscr{E}(x)\lambda}{2E_k}} .$$

The scattering rate per unit length, $1/\lambda$ (see Fig. 2), is corrected by a geometry factor which can be very large for the case of isotropic scattering (at low electron energies) in small electric fields.

For the calculation of the average $\langle z\rangle$ we need the distribution function of the scattering angles with respect to the field direction. However, we only know the distribution function for the scattering angles with respect to the incoming momentum of the electron. Yet at low energies the scattering is isotropic with respect to the incoming direction of the particle—and therefore also with respect to the field. At large energies the particles are forward directed and hence the incoming direction coincides roughly with the field direction. Taking the relevant distribution function to be the one known for the scattering angles should thus be a reasonable approximation.

At this stage we see that the balance between *gain* of energy by the field and *loss* by emission of LO phonons is a very delicate problem. For a donor density of $N_0=10^{18}$ cm^{-3} the initial field strength at the interface amounts to approximately 1.35 V/(100 Å) and the maximal loss at $E_k\sim0.2$ eV to ~0.15 eV/(100 Å). For a lower density $N_0=10^{16}$ cm^{-3} the gain lowers by a factor of 10 [approximately 0.135 V/(100 Å)] and the maximum loss rises to approximately 0.4 eV/(100 Å). The consequence of the change from dominant gain to dominant loss in the drift term is best illustrated by Fig. 3. Here we have plotted the distribution function for the (hot) electrons as a function of kinetic energy E_k for different positions x in the depletion region. The result for low donor density N_0, Fig. 3(a), shows that nearly all electrons are trapped in energy at the onset of LO-phonon scattering. As soon as the electrons pick up a tenth of an eV in the field, they fall back in energy by LO-phonon emission; hence, the electrons just roll down the potential hill. In Fig. 3(b), the electric field is large enough to overcome the bottleneck of large energy loss at small energies and all the electrons become hot. By suffering about ten scattering events they lose an energy of the order of 1 eV which is small compared to the gain of 4.5 eV in the field.

The second term in Eq. (3) describes the diffusion in energy space, i.e., the deviation from the average electron behavior discussed above. This diffusion leads to a broadening of the structure in the distribution function. The coefficient $\langle(\Delta E_k)^2\rangle/\Delta x$ is calculated by the path-integral method.

In the calculation we have taken account of acoustic phonon scattering and pair creation in the following way. The nature of acoustic phonon scattering allows for the idealization that scattering is negligible at low energies (small rate) but highly efficient in cooling at large energies (umklapp scattering, high rate). We are most interested in the high-energy tail of the distribution function, as this governs the total amount of pair creation. Electrons

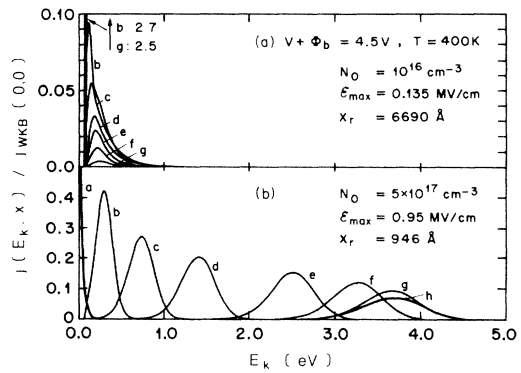

FIG. 3. Distribution function $j(E_k,x)$ versus kinetic energy E_k for different positions x in the depletion region: *a*, $x=0$; *b*, $x=x_0/25$; *c*, $x=x_0/10$; *d*, $x=x_0/5$; *e*, $x=2x_0/5$; *f*, $x=3x_0/5$; *g*, $x=4x_0/5$; and *h*, $x=x_0$. The injected tunneling current $j_{\rm WKB}(E_k,x)$ was calculated in the WKB approximation and the transmission coefficient for the purely thermionic current was taken unity. At the higher doping level, a fraction of approximately 0.3—0.5 of the electrons undergo an acoustic scattering event before arriving at x_0.

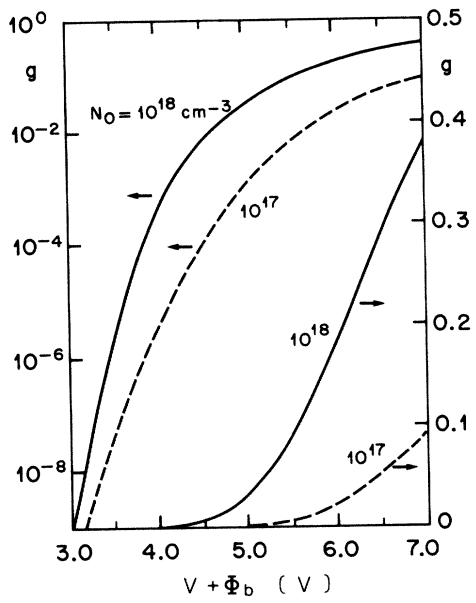

FIG. 4. Yield g for hole production as a function of the total potential drop $V+\Phi_b$ for two values of the donor density N_0.

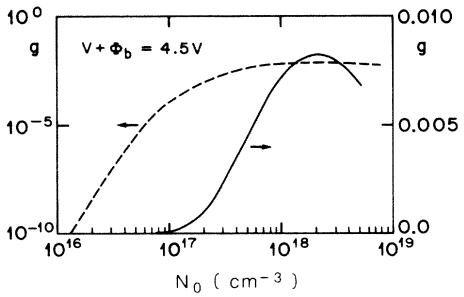

FIG. 5. Yield g for hole production versus donor density N_0 (electric field at the interface). At a density $N_0 \sim 10^{17}$ cm^{-3} the energy gain in the field becomes larger than the loss by LO-phonon scattering.

which have suffered an acoustic (umklapp) scattering event generally lose a larger amount of energy due to a significant path lengthening. Therefore they are taken out of the distribution by subtraction of a term

$$\frac{1}{\lambda_A(E_k)} j(E_k,x)$$

from the right-hand side of Eq. (3). Similarly, electrons which have created a pair lose more than $E_{\rm th}$ of their kinetic energy and are eliminated from the distribution function by subtraction of the term

$$\frac{1}{\lambda_I(E_k)} j(E_k,x) \,. \tag{4}$$

Finally integration of the term (4) supplies us with the desired *yield g* for the *hole production*

$$g=\frac{j_{\rm holes}}{j_{\rm in}}=\frac{1}{j_{\rm in}}\int dE_k \int dx \frac{1}{\lambda_I(E_k)} j(E_k,x) \,,$$

where $j_{\rm in}$ is the total incoming electron current. A plot of the yield g as a function of total potential energy $e\Phi_b+$eV at the interface (see Fig. 1) is shown in Fig. 4 for the two donor densities $N_0=10^{17}$ cm^{-3} and $N_0=10^{18}$ cm^{-3}. The yield depends strongly on the field strength in the depletion region (donor density N_0). This is illustrated in Fig. 5 where we plot g as a function of density N_0 for a fixed runway $e\Phi_b+$eV. For $N_0 \gtrsim 10^{17}$ cm^{-3} the yield rises steeply as the gain in the field starts to dominate the loss by LO-phonon emission. Note that g becomes large ($g>10^{-3}$) only for $e\Phi_b+$eV considerably larger than $E_{\rm th}$ which is approximately 3.7 eV in our example ($m_c=0.26m_e$, $m_v=1.5m_e$, $E_g=3.2$ eV, m_e is the free electron mass, Ref. 44).

III. STEADY STATE

The results of Sec. II show that it is possible to create holes within the depletion region of the grain boundary. These holes drift-diffuse back to the interface where they are trapped in the potential well. The holes do not become hot as easily as the electrons since: (i) their mobility is roughly a factor of 10 lower than the electron mobility for most II-VI compounds[45] and (ii) the electrons start with the maximum field at the interface which helps them to overcome the large loss at low energies, whereas the holes start in a region of low field. In the latter case the energy picked up in the field is then readily dissipated by the loss processes and it is much more difficult for the holes to get beyond the intense scattering region at low energies.

The hole *trapping* at the grain boundary must be balanced by a process in which holes *disappear* from the interface. This can occur either by *recombination* and/or by *emission* of holes over the barrier $e\Phi_b$ to the negatively biased side of the junction. Note that a recombined hole is lost as a screening charge for the negative interface charge, as the empty electron trap is immediately refilled.

In the calculation of the steady-state barrier Φ_b we must substitute the electronic interface charge Q_i, Eq. (2), by the total charge of electrons *and* holes. The total hole current arriving at the interface is proportional to the electron current j_r^e injected into the positively biased grain,

$$j^h=gj_r^e=g(j-j_{tl}^e+\tfrac{1}{2}j_{\rm em}^e) \,. \tag{5}$$

Here j is the thermally activated current

$$j=A^*T^2e^{-(e\Phi_b+\varepsilon_g)/k_BT}$$

and j_{tl}^e, $j_{\rm em}^e$ are the (electron) currents trapped at the interface,

$$j_{tl}^e=j\int dE\, c(E)N_i(E)[1-f_i(E)] \,, \tag{6}$$

and emitted out of the interface,

$$j_{\rm em}^e=\int dE\, b(E)e^{-(E_b-E)/k_BT}N_i(E)f_i(E) \,, \tag{7}$$

respectively.[14] The capture cross section $c(E)$ and the emission rate $b(E)$ are approximated by constants, which are related to one another by the detailed balance condi-

tion at $V=0$ ($b=2Ac$, $A=A^*T^2$, A^*=Richardson constant). The position of the bulk Fermi level relative to the conduction band is denoted by ε_ξ, and E_b is the top of the barrier, see Fig. 1. (We use the same notation as in BG throughout this paper.)

For the moment we assume with Pike[15] that the incoming hole current j^h is *fully trapped* and balanced by *electron-hole recombination* only. This of course affects the electronic interface charge Q^e, which we calculate now by determining the new quasi-Fermi-level at the interface. The rate equation for the electrons is

$$j_i^e = j_t^e - j_{\rm em}^e - j_{\rm rec}^e = 0$$

and the corresponding equation for the holes (no emission of holes) becomes

$$j_i^h = j^h - j_{\rm rec}^h = 0 \ . \tag{8}$$

Using these two equations and the equality of the two recombination currents $j_{\rm rec}^e = j_{\rm rec}^h = j_{\rm rec}$, we obtain the balance condition

$$j_t^e - j_{\rm em}^e - j^h = 0 \ .$$

Inserting Eqs. (5)–(7) we find the new expression for the *interface Fermi level* ξ_i, which is lowered by the recombination processes:

$$\Delta\xi = \xi - \xi_i = k_B T \ln\left[\frac{2+g}{1+e^{-eV/k_BT} - g_c}\right] , \tag{9}$$

with

$$g_c = g\frac{1-\hat{c}}{\hat{c}}, \quad \hat{c} = c\int dE\, N_i(E)[1-f_i(E)] \ .$$

Inserting this new expression for ξ_i into Eq. (2) the electronic interface charge Q^e can be calculated.

The above calculation works for the single-level interface DOS as well as for the continuous DOS in the perfectly relaxing model, where the occupation of the interface traps is described by a Fermi function. The model with localized interface states needs some additional ideas which are described in Appendix A.

Next we have to calculate the steady-state hole charge Q^h present at the interface. The latter is determined by the hole rate equation (8) and the ansatz for the recombination current $j_{\rm rec}$,

$$j_{\rm rec} = \frac{r}{e} Q^e Q^h \equiv \frac{1}{\tau_r} Q^h \ ,$$

Using Eqs. (5)–(9) leads to the result

$$Q^h = gj\tau_r \frac{2-\hat{c}}{2+g} \ . \tag{10}$$

The total interface charge $Q_i = Q^e - Q^h$ must be calculated *self-consistently* with the barrier Φ_b. This is a rather tricky numerical problem which was solved in the following way. For a given applied bias V across the grain boundary we start with a guess for the barrier Φ_b [$\rightarrow g = g(V+\Phi_b)$]. In an inner loop we determine self-consistently the interface charge Q^e which depends on the trapping probability $\hat{c}(Q^e)$ through the quasi-Fermi-level ξ_i, Eq. (9). In the outer loop we then improve the value for the barrier Φ_b. This second iteration is illustrated in Fig. 6 where we plot the new barrier Φ_b as a function of the old value of Φ_b for the two cases with and without hole generation.

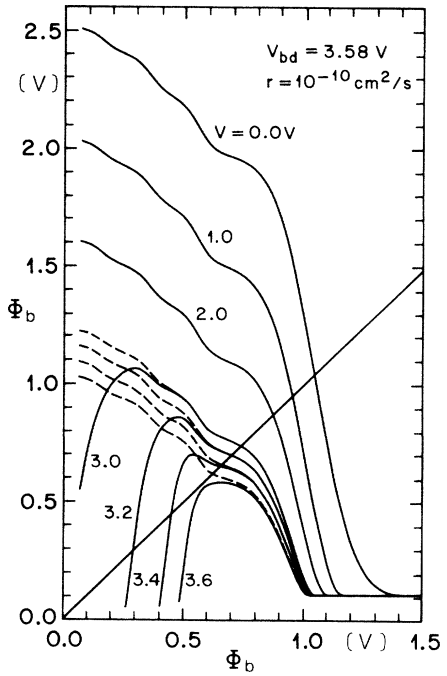

FIG. 6. Self-consistency plot for the barrier Φ_b for different values of applied bias V. Comparison is made for the two situations with (solid lines) and without (dashed lines) hole creation. Without holes, only one solution for Φ_b exists for a given bias V. The accumulation of holes bends the curves down at large bias, such that two values for Φ_b are found for a given V. These two solutions are the barrier heights before (large Φ_b) and after (small Φ_b) breakdown. No self-consistent value for Φ_b can be found for a bias V exceeding the breakdown voltage V_{bd}.

In order to discuss the complete model we always show the results for the general case where deep bulk traps are present. The inclusion of these traps into the above formulas is straightforward [only Φ_b, Eq. (1), undergoes a slight change]. The same data as in our previous paper (BG) have been used. A Gaussian interface DOS, positioned 2 eV above the valence-band edge, with a trap density $N_i = 10^{13}$ cm^{-2} and a width of $\Delta E = 0.15$ eV; a shallow donor 20 meV below the conduction band E_c with density 10^{18} cm^{-3} and three deep bulk traps at energies 0.2, 0.4, and 0.6 eV below E_c with densities 5×10^{16} cm^{-3}, 1×10^{17} cm^{-3}, and 2×10^{17} cm^{-3}. The capture cross section of the interface states is $c = 10^{-13}$ cm^2 and the values for the bulk states are all 10^{-14} cm^2. The temperature has been chosen $T=400$ K and the dielectric constant is $\epsilon=9$. Further, we have used a grain conductivity of 10.8 S/cm for a grain size of 15 μm. The Fermi level is at $\varepsilon_\xi = 67$ meV below E_c and the Richardson constant amounts to 30 A cm^{-2}K^{-2}.

The most prominent feature in Fig. 6 is the rapid decay of the barrier Φ_b in the presence of holes. A reduction in

Φ_b enhances the injected electron current j_r^e and consequently also the hole charge Q^h exponentially. This leads to a *barrier-controlled avalanche breakdown* manifested in the fact that the grain boundary bias V cannot exceed a critical value V_{bd}. After reaching this value from below, the grain boundary bias V shrinks again such that $g(V+\Phi_b)$ is reduced sharply, thereby compensating the growth in j_r^e. Consequently we find a *negative differential resistance* up to the point where the current flowing across the grain boundary is limited by the finite conductivity of the grains. This new type of bistability has not been reported in the literature before.

In Fig. 7 we illustrate the behavior of the barrier Φ_b and of the total interface charge Q_i as a function of the applied *external* bias $V_{\text{grain}}=V+V_{\text{bulk}}$ (V_{bulk} is the potential drop within the bulk of one grain). Again we compare the situations with and without hole generation. At about 3.6 V the critical bias V_{bd} is reached where the barrier-controlled avalanche breakdown sets in as described above ($g\sim 10^{-3}$). The breakdown voltage V_{bd} depends on g and on the recombination parameter r for which we have chosen the value $r=10^{-10}$ cm^2/s. This leads to a recombination time $\tau_r=1$ ms, a value well within the range of e-h recombination times reported in the literature[46] (values are found ranging over several orders of magnitude from picoseconds to seconds). A decrease of τ_r by a factor of 100 leads to an increase of the breakdown voltage V_{bd} by approximately 0.5 V, see Fig. 7. A comparison of V_{bd} with the experiments can be used to get an estimate for the recombination time τ_r at the interface, a quantity which is not easily accessible by experiment otherwise.

The collapse of the barrier in the presence of holes is completed by a relatively small reduction in interface charge: after a decrease of Q_i by roughly one-third, the further decay of the barrier is limited by the finite conductivity of the grains. This reduction of Q_i is due to the

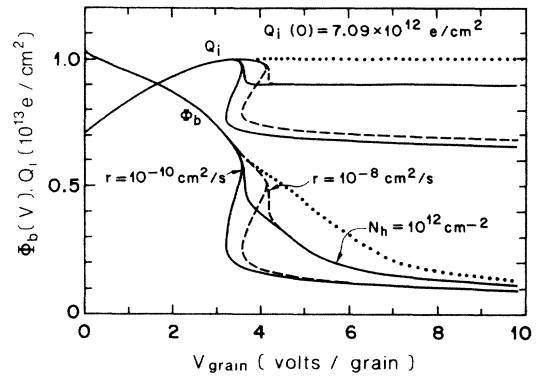

FIG. 7. Barrier height Φ_b and interface charge Q_i versus external bias V_{grain}. We compare the calculation without holes (dotted lines) with the situation where holes are accumulated using a finite ($N_h=10^{12}$ cm^{-2}) and an infinite hole density. In the latter case a pronounced instability is developed. The breakdown of the barrier depends on the recombination parameter r as well as on the capture cross section c_h ($c_h=10^{-12}$ cm^2).

accumulation of holes Q^h alone. The lowering of the Fermi level, as a consequence of the recombination processes described by Eq. (9) is only of minor importance; although, in the present case, $\Delta\xi$ increases by a factor of 4, this growth is more than compensated by the decrease of Φ_b, such that the electron states are always nearly filled (note that g_c approaches 1 but is always bounded by 1).

We have tried to modify the model described above in order to find a way around the instability created by the strong hole accumulation. A first possibility is the introduction of a *finite density of hole states* N_h at the interface in close analogy to the finite number of electron traps. The total hole flux is then divided up into a fraction trapped at the grain boundary

$$\hat{c}_h=c_h N_h(1-f_h)=c_h(N_h-Q^h/e)$$

(c_h is the capture cross section and f_h is the occupation probability), and a second part which is emitted into the negatively biased grain. We will neglect this latter contribution to the total current as its magnitude is small.

The hole rate equation is changed to

$$j_i^h=\hat{c}_h j^h-j_{\text{rec}}^h=0\ .$$

In the shift of the interface Fermi level ξ_i, Eq. (9), we simply have to substitute g by $\hat{g}=g\hat{c}_h$.

The hole charge Q^h, Eq. (10), takes the new form[47]

$$Q^h=\frac{\lambda}{1+\lambda}eN_h,\quad \lambda=gj\tau_r\frac{c_h}{e}\frac{2-\hat{c}}{2+\hat{g}}\ .$$

The result of a calculation using the density $N_h=10^{12}$ cm^{-2} and the capture cross section $c_h=10^{-12}$ cm^2 is shown in Fig. 7 for two values of the recombination parameter r. The limitation of the hole charge Q^h prevents the barrier from becoming instable. The old results are reproduced in the limit of an infinite density of donor states $N_h\to\infty$, $N_h c_h=1$.

A second way to eliminate the instability is to assume *thermal emission of holes* over the barrier Φ_b into the negatively biased grain. We have performed a model calculation which treats electrons and holes at the interface identically. The recombination rate was set equal to zero and substituted by the emission process which increases exponentially as the barrier Φ_b is lowered. This leads to a rapid and stable decay of the barrier Φ_b which we illustrate in Fig. 8 for a reasonable set of parameters (single-level densities $N_h=10^{12}$ cm^{-2}, 10^{13} cm^{-2} at $E_h=0.2$ eV, 0.4 eV above the valence band, and charge emission rate $b_h=10^{-7}$ A). The exponentially growing hole production with decreasing barrier Φ_b is compensated by the exponential rise in hole emission from the interface. This compensation reduces the sharp growth in Q^h which otherwise would lead to the instability.[48]

The emission-only model however suffers from the deficiency that it cannot explain the negative small-signal capacitance at large bias found experimentally (see below). In a complete model probably both effects, hole recombination and emission, must be taken into account. We do

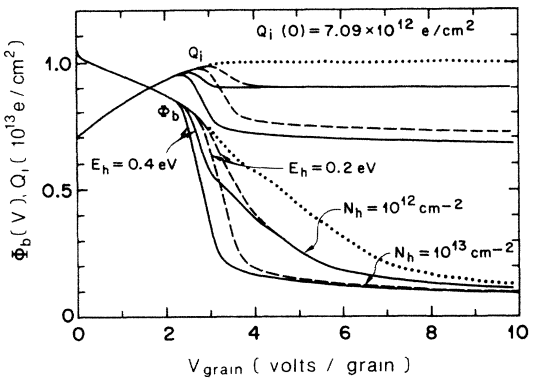

FIG. 8. Barrier height Φ_b and interface charge Q_i versus external bias V_{grain} for the emission-only model. Comparison to the case without holes is made (dotted lines). Again two hole densities, $N_h = 10^{12}$ cm^{-2} and $N_h = 10^{13}$ cm^{-2} ($c_h N_n = 1$), are considered. The dependence on the trap position E_h is studied. An increase of E_h corresponds to a reduction in hole emission and the breakdown of the barrier is initialized at a lower bias.

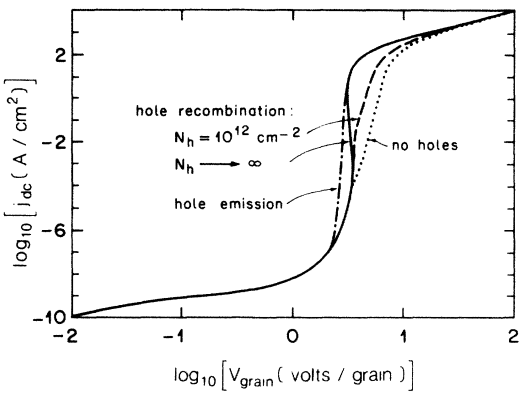

FIG. 10. dc current j_{dc} versus applied bias V_{grain}. The stable behavior for the cases where no holes are present (dotted line), or where the hole density is limited (dashed line—hole recombination; dashed-dotted line—hole emission) is contrasted with the instability found for the model where all holes are accumulated at the interface.

not think, however, that performing this very involved calculation (the dynamics becomes very complicated) will bring many new insights, besides adding also more parameters to the model.

In the upper breakdown region the current across the sample is limited not only by the grain-boundary barriers alone. This is shown in Fig. 9 where we plot the voltage drop V across the interface as a function of the total applied (external) bias V_{grain} for the various models presented above. As the barrier decays beyond approximately 0.2 V the finite conductivity of the grains becomes dominant.

The behavior of the *external current* j_{dc}, which is thermally activated over the barrier, is illustrated in Fig. 10:

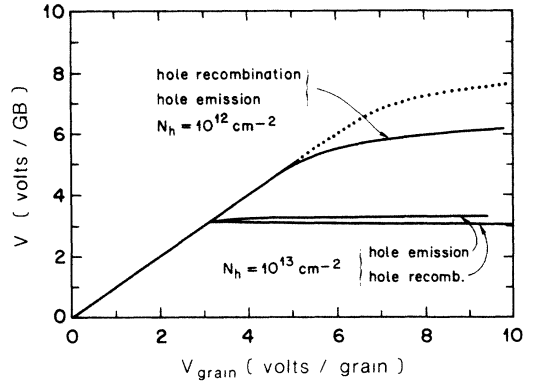

FIG. 9. Voltage drop V across the grain boundary (GB) versus external bias V_{grain} for the models (i) with no holes (dotted line), (ii) with a small hole density $N_h = 10^{12}$ cm^{-2} considering both, hole recombination or hole emission, and (iii) with a large hole density $N_h = 10^{13}$ cm^{-2} or $N_h \to \infty$, considering again hole emission or hole recombination. As the barrier drops below approximately 0.2 V the total applied bias V_{grain} is divided up into a voltage drop V across the junction and a potential loss through the ohmic grain $V_{grain} - V$.

$$j_{dc} = j(1 - e^{-eV/k_B T}) - \tfrac{1}{2} j_{em} + j_{rt} ,$$

$$= j\left[1 - \frac{\hat{c}}{2}\right]\left[1 + \frac{\hat{g}}{2+\hat{g}}\right](1 - e^{-eV/k_B T}) .$$

Again we compare the new results with the case where no holes are generated. An S-shaped instability is formed when the growth of the hole charge Q^h is not limited by a finite N_h. This leads to a divergence of the nonlinearity coefficient $\alpha = d(\ln j)/d(\ln V)$ at $V = V_{bd}$. For the case of a finite hole density N_h the current j rises steeply as the barrier decays, but remains well behaved. The nonlinearity parameter α shown in Fig. 11 develops a sharp peak when the holes accumulate at the interface. α values well beyond approximately 100 are reached, depending on the model parameters. The fine structures in Figs. 6—11 are

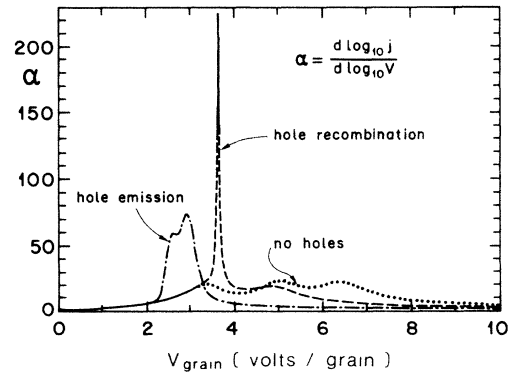

FIG. 11. Nonlinearity parameter α versus applied bias V_{grain} for the grain-boundary models of Fig. 10. For the bistable case (not shown) α diverges as V approaches V_{bd}, and becomes negative and diverges again as the negative differential resistance turns positive for the second time.

due to the neutralization of the deep bulk traps as discussed in BG.

In the calculation of the electrical response we describe the transport over the barrier Φ_b by the thermionic emission model. The results of Sec. II show that a true description should take into account the scattering processes in the depletion region. However the small number of scattering events renders the thermionic emission model reasonable. Furthermore the description of transport by a diffusion model only changes the prefactor in j but not the exponential dependence on the barrier Φ_b.

IV. TIME-DEPENDENT PROPERTIES

In this section we calculate the time-dependent properties of the carrier transport in linear-response theory. As an illustration we treat the simplest case of a single-level DOS for the electronic interface traps and no deep bulk defects. The number of holes at the interface is determined by e-h recombination. The density of hole traps at the interface is taken as finite, since it is easy to generalize the results to the case where all holes are trapped. The models with a continuous DOS for the interface are treated in Appendixes B and C.

The calculation runs along the same lines as in the previous publication (BG). The application of a time-dependent bias across the grain boundary,

$$V(t)=V_0+\tilde{V}e^{i\omega t},\quad e\tilde{V}\ll k_BT\ ,$$

leads to the variation of the interface charges Q^e and Q^h, as well as of the screening charge in the depletion regions. This (time-delayed) response results in a modulation of the barrier Φ_b which in turn exponentially modulates the current measured across the junction. A second contribution to the total current flowing through the interface is the displacement current generated by the charge transfer between the two depletion regions. The study of the time-dependent current can be used to determine the microscopic parameters of the states involved in the current transport.

We start with the calculation of the *dynamics of the hole charge* Q^h, which is determined by the rate equation[49]

$$i\omega\tilde{Q}^h e^{i\omega t}=\frac{dQ^h}{dt}=j_t^h-j_{\rm rec}^h=(\tilde{j}_t^h-\tilde{j}_{\rm rec}^h)e^{i\omega t}\ . \tag{11}$$

By expansion of the hole current trapped at the interface we find[50]

$$\tilde{j}_t^h=\hat{g}_0 j_0\left[\frac{e}{k_BT}(1-\hat{c}_0)\tilde{\Phi}_b+\left[\frac{\hat{c}_0}{1-f_{i0}}+\frac{\hat{c}_0}{f_{i0}}\frac{1-\hat{g}_{0c}}{2+\hat{g}_0}\right]\tilde{f}_i+\frac{g_0'}{g_0}\frac{2-\hat{c}_0}{2+\hat{g}_0}(\tilde{V}-\tilde{\Phi}_b)\right]-\frac{\lambda_0}{\tau_{r0}}\tilde{Q}^h \tag{12}$$

and the expansion of the recombination current $j_{\rm rec}^h$ leads to

$$\tilde{j}_{\rm rec}^h=\frac{1}{\tau_{r0}}\left[\tilde{Q}^h+\frac{Q_{i0}^h}{f_{i0}}\tilde{f}_i\right]\ . \tag{13}$$

The index "0" indicates the steady-state value of this quantity. We have introduced the derivative g_0' of the yield g at $V_0+\Phi_{b0}$. Note that the hole charge Q_0^h may still be expressed as [compare Eq. (10)]

$$Q_0^h=\hat{g}_0 j_0\tau_{r0}\frac{2-\hat{c}_0}{2+\hat{g}_0}$$

also in the case of a finite hole density.

Inserting of Eqs. (12) and (13) into the rate equation (11) determines $\tilde{Q}^h$,

$$\tilde{Q}^h=\frac{\hat{g}_0 j_0\tau_{r0}}{1+\lambda_0+i\omega\tau_{r0}}\left[\frac{e}{k_BT}(1-\hat{c}_0)\tilde{\Phi}_b+\frac{g_0'}{g_0}\frac{2-\hat{c}_0}{2+\hat{g}_0}(\tilde{V}-\tilde{\Phi}_b)+\left[\frac{\hat{c}_0}{1-f_{i0}}-\frac{1-\hat{c}_0}{f_{i0}}\right]\tilde{f}_i\right]\ . \tag{14}$$

In a next step we calculate the *modulation of the electronic interface charge* Q^e, which is governed by the rate equation

$$i\omega\tilde{Q}^e e^{i\omega t}=\frac{dQ^e}{dt}=j_t^e-j_{\rm em}^e-j_{\rm rec}^e=(\tilde{j}_t^e-\tilde{j}_{\rm em}^e-\tilde{j}_{\rm rec}^e)e^{i\omega t}\ .$$

Expansion of $j_t^e-j_{\rm em}^e$ leads to the result

$$\tilde{j}_t^e-\tilde{j}_{\rm em}^e=j_0\frac{e\hat{c}_0}{k_BT}(1+e^{-eV_0/k_BT})\times\left[\tilde{\Phi}_b-\frac{\tilde{V}}{1+e^{eV_0/k_BT}}-\frac{k_BT}{e}\left[\frac{1}{1-f_{i0}}+\frac{2}{f_{i0}}\frac{1-\hat{g}_{0c}}{2+\hat{g}_0}\right]\tilde{f}_i\right]$$

and $\tilde{j}_{\rm rec}^e=\tilde{j}_{\rm rec}^h=\tilde{j}_{\rm rec}$ is given by (13). The dynamics of the total interface charge Q_i then is given by the solution of the equation

$$i\omega(\tilde{Q}^e-\tilde{Q}^h)=\tilde{j}_t^e-\tilde{j}_{\rm em}^e-\tilde{j}_t^h\ . \tag{15}$$

We first use Eq. (15) to determine the modulation $\tilde{f}_i$,

$$\tilde{f}_i=\frac{e}{k_BT}f_{i0}(1-f_{i0})\times\frac{(1+\vartheta_r-\hat{g}_{\rm ocr})\tilde{\Phi}_b-\left[\vartheta_r+\frac{1}{1+e^{eV_0/k_BT}}\right]\tilde{V}}{1+\mu+i\omega\tau_i}\ .$$

Here we have introduced the abbreviations

$$\hat{g}_{\rm ocr}=\hat{g}_{0c}\frac{1}{1+\lambda_0+i\omega\tau_{r0}}\ ,$$

$$\vartheta_r=\hat{g}'_0\frac{k_BT}{e\hat{c}_0}\frac{2-\hat{c}_0}{2+\hat{g}_0}\frac{1}{1+\lambda_0+i\omega\tau_{r0}},\quad \bar{\vartheta}_r=\frac{\vartheta_r}{1-\hat{g}_{0cr}},$$

and

$$\mu=\hat{g}_{0r}\left[1-\frac{1}{cN_i}\right],\quad \hat{g}_{0r}=\hat{g}_0\frac{1}{1+\lambda_0+i\omega\tau_{r0}}.$$

The expression for the interface relaxation time τ_i is[14]

$$\tau_i=\frac{ef_{i0}}{Ac}\frac{1}{1+e^{-eV_0/k_BT}}e^{(e\Phi_{b0}+\varepsilon_\xi)/k_BT}=f_{i0}\tau'_i.$$

The exponential dependence on $\Phi_{b0}(V_0)$ allows τ_i to vary over several orders of magnitude.

Inserting the result for $\tilde{f}_i$ into Eq. (15) we find the modulation of the interface charge Q_i,

$$\tilde{Q}_i=C_i^{\Phi}(\omega)\tilde{\Phi}_b-C_i^{V}(\omega)\tilde{V},$$

with the capacitances

$$C_i^{\Phi}(\omega)=C_i^e(\omega)\left[1+\lambda_0\hat{g}_{0cr}-\hat{g}_{0c}-\frac{\tau_{r0}}{\tau'_i}\frac{\hat{g}_{0r}}{\hat{c}_0}+\vartheta_r\left[1+\frac{\tau_{r0}}{\tau_i}+i\omega\tau_{r0}\right]\right],$$

$$C_i^{V}(\omega)=C_i^e(\omega)\left[\frac{1}{1+e^{eV_0/k_BT}}+\vartheta_r\left[1+\frac{\tau_{r0}}{\tau_i}+i\omega\tau_{r0}\right]\right],$$

and

$$C_i^e(\omega)=\frac{e^2\hat{c}_0}{ck_BT}f_{i0}\frac{1}{1+\mu+i\omega\tau_i}.$$

We proceed with the calculation of the *time dependence of the barrier height* Φ_b. We can relate $\tilde{\Phi}_b$ to the variation of the screening charges $Q_{l0}=eN_0x_{l0}$ and $Q_{r0}=eN_0x_{r0}$,

$$-\tilde{\Phi}_b=\frac{\tilde{Q}_{l0}}{C_l}=\frac{\tilde{Q}_{r0}}{C_r}-\tilde{V},$$

where we have introduced the capacitances $C_l=\epsilon_0\epsilon/x_{l00}$ and $C_r=\epsilon_0\epsilon/x_{r00}$. All charge modulations $\tilde{Q}_i$, $\tilde{Q}_{l0}$ and $\tilde{Q}_{r0}$ can now be expressed as a function of $\tilde{\Phi}_b$ and $\tilde{V}$. The charge-neutrality condition

$$Q_i(t)=Q_{l0}(t)+Q_{r0}(t)$$

allows one then to relate $\tilde{\Phi}_b$ to the known amplitude $\tilde{V}$

$$\tilde{\Phi}_b=\frac{C_r+C_i^{V}(\omega)}{C_r+C_l+C_i^{\Phi}(\omega)}\tilde{V}.$$

Finally we determine the *current* through the junction, which is made up of an injection part and a displacement part. We calculate the thermionic injection current (on the left-hand side of the barrier)

$$j_{lb}=j(1-e^{-eV/k_BT})+j_{rt}-\tfrac{1}{2}j_{em}$$

in linear response and find the result

$$\tilde{j}_{lb}=\sigma_0\left[\left[1-\frac{\bar{\vartheta}_r}{2/\eta\hat{c}_0-1}-e^{-eV_0/k_BT}\right]\tilde{\Phi}_b+\left[\frac{\bar{\vartheta}_r}{2/\eta\hat{c}_0-1}+e^{-eV_0/k_BT}\right]\tilde{V}\right]$$

$$+\sigma_i(\omega)\left[(1+\bar{\vartheta}_r)\tilde{\Phi}_b-\left[\bar{\vartheta}_r+\frac{1}{1+e^{eV_0/k_BT}}\right]\tilde{V}\right].$$

The conductance σ_0 is a slight modification of the zero-bias dc conductance (where $\eta=1$),

$$\sigma_0=j_0\frac{e}{k_BT}\left[1-\frac{\hat{c}_0}{2}\eta\right],\quad \eta=\frac{(1-\hat{g}_{0c})(1-\hat{g}_{0cr})}{1+\hat{g}_0/2},$$

and $\sigma_i(\omega)$ is

$$\sigma_i(\omega)=j_0\frac{c}{2e}\eta C_i^e(\omega)\left[(1+i\omega\tau'_i)-e^{-eV_0/k_BT}(1-i\omega\tau'_i)+\frac{\mu}{f_{i0}}\right].$$

The displacement current $j_{ld}=-\dot{Q}_{l0}$ adds the contribution

$$\tilde{j}_{ld}=i\omega C_l\tilde{\Phi}_b.$$

The total ac small-signal current finally is

$$j_{ac}=\sigma\tilde{V}e^{i\omega t}$$

with the *admittance* σ,

$$\sigma=\left[\left[1-\frac{\bar{\vartheta}_r}{2/\eta\hat{c}_0-1}-e^{-eV_0/k_BT}\right]\sigma_0+(1+\bar{\vartheta}_r)\sigma_i(\omega)+i\omega C_l\right]\frac{C_r+C_i^V(\omega)}{C_r+C_l+C_i^\Phi(\omega)}$$
$$+\left[\left[\frac{\bar{\vartheta}_r}{2/\eta\hat{c}_0-1}+e^{-eV_0/k_BT}\right]\sigma_0-\left[\bar{\vartheta}_r+\frac{1}{1+e^{eV_0/k_BT}}\right]\sigma_i(\omega)\right]. \quad (16)$$

Before discussing this main result, let us say a few words concerning the generalizations of Eq. (16): If all holes produced in the depletion region are trapped at the interface, we can simply use (16) after taking the limit $N_h\to\infty$, $c_hN_h=1$. This corresponds to setting $\hat{c}_{h0}=1$ and $\lambda_0=0$.

The presence of deep bulk traps is taken into account very easily by substituting the depletion region capacitances C_l and C_r by their updated values including the deep traps. Some care has to be taken, as the denominator of $\tilde{\Phi}_b/\tilde{V}$ picks up an additional capacitance whenever a deep trap gets neutralized completely as it drops below the quasi-Fermi-level. For details we refer to our previous publication BG.

The behavior of the admittance σ as a function of applied bias V, frequency ω, and temperature T has been thoroughly discussed in BG. Here we will concentrate on the new phenomena introduced by the presence of holes at the interface. Most of the g-dependent terms in σ are only minor corrections to the previous result in BG. The major change is introduced by the terms

$$-\hat{g}_{0c}-\frac{\tau_{r0}}{\tau_i'}\frac{\hat{g}_{0r}}{\hat{c}_0} \quad (17)$$

in the interface capacitance $C_i^\Phi(\omega)$.

The total *capacitance*

$$C=\frac{1}{\omega}\mathrm{Im}\sigma$$

of the junction consists of a contribution from the displacement current j_{ld} and a second contribution which has its origin in the time-delayed response of the interface charge. This time delay is transferred to the barrier Φ_b and therefore the injected current is shifted in phase, hence generating a capacitive component.

The displacement current part is given approximately by the high-frequency (hf) capacitance

$$C_{\mathrm{hf}}(V_0)=\frac{\epsilon_0\epsilon}{x_{l00}(V_0)+x_{r00}(V_0)}$$

(plus smaller corrections when deep traps are present).

The second part (injected current) depends strongly on bias V_0 and frequency ω: For $\omega\tau_i(V_0)>1$ the interface charge does not follow the applied ac signal and no capacitance is developed. As V_0 increases the relaxation time $\tau_i(V_0)$ decreases and $\omega\tau_i(V_0)$ falls below 1. The time-delayed charging and discharging of the interface then introduces a large capacitive effect which we illustrate in Fig. 12. (Throughout all plots, we use for the junction the parameters given in Sec. III, including the deep bulk traps.) As all interface states become filled at large bias, the capture probability $\hat{c}_0$ approaches zero and the interface capacitance $C_i^e(\omega)$ disappears. However, when holes are present, an additional relaxation process is introduced

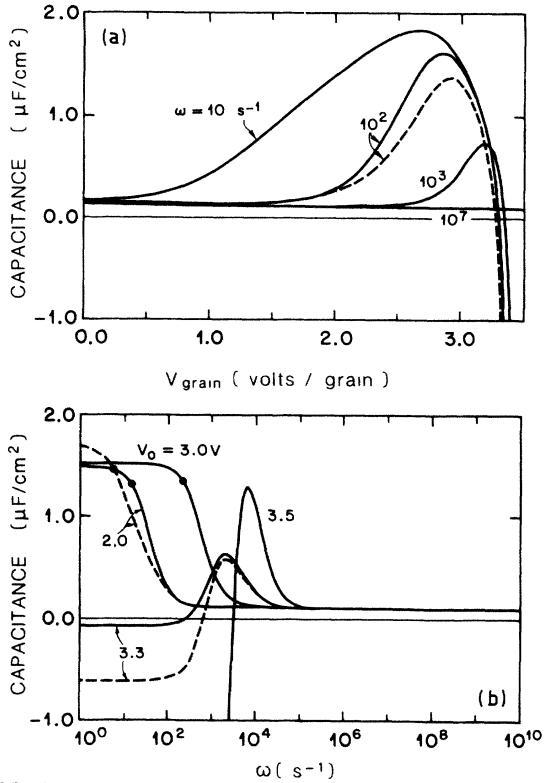

FIG. 12. (a) Capacitance C versus external bias V_{grain} for the model with a finite density of hole traps and hole recombination ($N_h=10^{12}$ cm^{-2}, $r=10^{-10}$ cm^2/s, steady state see Figs. 7 and 9–11). We take a continuous (Gaussian) interface DOS and assume perfect relaxation among the electron traps. The capacitance becomes negative at a bias $V_{\mathrm{grain}}\sim 3.3$ V considerably lower than the voltage needed to suppress the barrier, $V_{\mathrm{grain}}\sim 3.6$ V. For comparison we also show the result for the same DOS, but treating the electrons at the interface as completely localized (dashed line). (b) Capacitance C versus frequency ω. At low frequencies the time-delayed charging and discharging of the interface produces a large capacitance which disappears when the interface cannot follow the signal any longer. At high bias V_0 the hole dynamics dominates and the capacitance turns to negative values. The dashed lines are the comparison to the model with localized states.

by the e-h recombination. The latter does not disappear when the interface is filled [the terms in (17) are both proportional to $1/\hat{c}_0$] and has an *opposite sign* as its origin is the hole charge Q^h in Q_i. With increasing bias V_0, the term

$$-\frac{\tau_{r0}}{\tau_i'}\frac{\hat{g}_{0r}}{\hat{c}_0}$$

grows in magnitude (decrease of τ_i') and finally, when the dominant relaxation process has shifted from the electrons to the holes, the capacitance $C_i^{\Phi}(\omega)$ becomes negative. As $C_i^{\Phi}(\omega)$ is much larger in magnitude than the depletion region capacitance C_l+C_r, the sign of the total capacitance C is reversed simultaneously. Since $\hat{g}_{0r}$ depends on ω, the whole process is frequency dependent. An increase in ω shifts the sign reversal of C to larger bias values [see Fig. 12(a)].

The frequency dependence of the capacitance is illustrated in Fig. 12(b). For large bias V_0 the capacitance becomes negative at small values of ω.

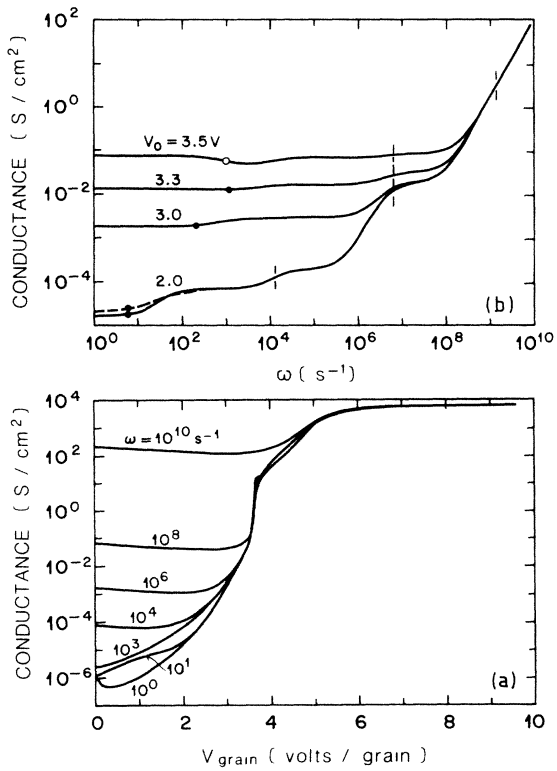

FIG. 13. (a) Conductance G versus external bias V_{grain}. The presence of deep bulk traps leads to the large zero bias dispersion. The sharp decay of the barrier around $V_{\text{grain}}\sim 3.6$ V is responsible for the strong increase in G. At large bias the conductance is dominated by the ohmic grains. (b) Conductance G versus frequency ω. The voltage-dependent resonances at low frequencies are due to the interface. For $V_0=3.5$ V the hole dynamics leads to a resonance with a reversed character (open circle). At large frequencies the displacement current dominates and the bulk trap resonances are clearly visible. For $\omega \gtrsim 10^8\ \text{s}^{-1}$ the finite conductivity of the grains cannot be neglected: The balance between conductance and capacitance is altered in favor of the conductance. The dashed line is again the comparison to the model with localized states.

For the sake of completeness we also present plots of the *conductance* $G=\text{Re}\sigma$ as a function of bias V_{grain} [Fig. 13(a)] and as a function of frequency ω [Fig. 13(b)]. A sharp rise in $G(V_{\text{grain}})$ indicates the hole-induced breakdown. At low bias the large dispersion added by the deep traps is dominant [Fig. 13(a)]. In Fig. 13(b) the decrease in G for $V_0=3.6$ eV is due to the resonant electron-hole recombination process (note the reversed sign of this resonance as compared to the electronic interface resonance at small bias values). The high-frequency part of the plot differs from the result previously published, (BG) as we have included the finite conductivity of the grains in the present calculation.

The above calculations treat the case of a single-level DOS for the electron traps at the interface. The formulas experience only minor changes for the more general case of a continuous DOS in the relaxing model (compare this to the results in Appendix B). The case of perfectly localized states is much more complicated to calculate and the final results look quite different. A numerical evaluation, however, proves that the differences between the two relaxation models for a continuous DOS are only of minor importance (see Figs. 12 and 13), a result which we have already discussed in BG.

Finally we also performed a calculation where the holes disappear from the interface by emission processes instead of recombination with electrons. This model suffers from the drawback that it does not lead to a negative capacitance for a meaningful set of parameters, although the steady-state breakdown looks reasonable (see Fig. 8). The main reason is that the leading parts of the hole creation and emission currents are in phase and of equal magnitude (detailed balance) in this model, because both processes are governed by the same barrier Φ_b. Therefore no large (negative) hole capacitance is induced.

V. CONCLUSION

We have calculated the steady-state and time-dependent behavior of majority carrier transport through grain boundaries for the case where large electric fields at the interface play a dominant role. We have shown that electrons can pick up a large amount of kinetic energy if the field is strong enough. The main hindrance for the electrons to become hot is the strong, isotropic polar optical-phonon scattering at low carrier energies. Once the electrons have overcome this bottleneck, the scattering becomes forward directed with increasing energy and the electrons become hot. Increasing the doping concentration leads to a higher electric field at the interface, thereby favoring hot carrier generation and the subsequent production of holes by impact ionization.

The holes, which drift-diffuse back to the interface, have a severe effect on the stability of the potential barrier. Trapping of all holes at the interface leads to a barrier-controlled avalanche breakdown and a negative differential resistance region in the current-voltage characteristics, as long as electron-hole recombination is the only process of hole-charge regulation at the interface.

If the total hole charge is limited by a finite trap density, it becomes possible to get rid of the bistability. Another way to find a unique barrier Φ_b at breakdown is to substitute the electron-hole recombination by hole emission, however in this case no negative capacitance could be found.

The present calculations show a negative small-signal capacitance at large bias, where the modulation of the barrier is dominated by the hole-charge dynamics (model with *e-h* recombination at the interface). This negative capacitance is interpreted in the following way: At moderate bias values, where the electron interface states play the dominant role, a lowering of the barrier is followed by an increased electron trapping ($dQ_i/dV>0$), as empty electron traps are shifted below the Fermi level ξ_i. This stabilizing charge accumulation lags behind in time, thereby giving rise to a (positive) capacitive component in the modulated over-barrier current. With increasing bias the interface states for the electrons are filled and the stabilization effect dies away as the electron charge Q^e remains at its maximum value—the capacitance decreases.[51] As the barrier is lowered further, holes are created in the depletion region and a positive interface charge Q^h is built up. A lowering of the barrier is followed by an increase in hole production and therefore in Q^h. The barrier is destabilized ($dQ_i/dV<0$) and the capacitance goes in the opposite (negative) direction. Such a negative capacitance has indeed been observed at ZnO (Refs. 13, 15, and 52) and GaAs (Ref. 16) grain boundaries. The above theoretical considerations give a deeper understanding of this phenomenon.

With the complete model presented here, it now becomes possible to thoroughly analyze the experimental data. Some care must be taken at very large bias (upper breakdown region) where only pulsed measurements and no admittance data are available. On the experimental side it becomes difficult therefore to identify a bistability. On the other hand, at these high voltages (i.e., for $\phi_b \to 0$), both effects, electron-hole recombination as well as hole emission, probably should be considered simultaneously for an accurate fit. However, we do not expect to find new insights from such a calculation. Both, theory and experiment yield reliable data in the prebreakdown and the lower breakdown region: steady-state characteristics and dynamic response as a function of bias, frequency, and temperature. These data allow the verification of the model and the determination of the underlying microscopic parameters.

ACKNOWLEDGMENTS

The authors wish to thank J. Bernasconi, C. G. Günther, M. Rossinelli, and G. E. Pike for many helpful discussions. Special thanks go to D. Baeriswyl for his many inspiring discussions concerning the hot-electron problem.

APPENDIX A

We determine the *steady-state* occupation statistics for a continuous interface DOS $N_i(E)$ in the limit where the electrons are *localized* within the interface. The interface is then in thermal equilibrium only by exchange with the bulk. No equilibration among the interface states is allowed. The detailed balance condition has to be evaluated for each level separately. The rate equation for each electron level is

$$j_i^e = j_t^e - j_{\rm em}^e - j_{\rm rec}^e \tag{A1}$$

and the analog equation for the holes is

$$j_i^h = j_t^h - j_{\rm rec}^h \,. \tag{A2}$$

The two recombination currents $j_{\rm rec}^e$ and $j_{\rm rec}^h$ are not identical any longer as we have to take $j_{\rm rec}^e$ for a single level only,

$$j_{\rm rec}^e = \frac{r}{e} Q^e Q^h \,,$$

whereas the holes recombine with all electron states,

$$j_{\rm rec}^h = \frac{r}{e} Q^h \int dE\, Q^e(E) \equiv \frac{r}{e} Q^h Q^{e,t} \,.$$

Analogously the hole current j^h contains a contribution of all electron states,

$$j^h = g\left[j(1-\hat{c}) + \tfrac{1}{2} b \int dE\, N_i f_i e^{-(E_b - E)/k_B T} \right] .$$

Evaluation of the detailed balance condition in the presence of holes,

$$j_t^e = j_{\rm em}^e + j_{\rm rec}^e$$

leads to the result

$$f_i = \frac{1}{1+\chi+e^{(E-\xi_i)/k_B T}} \,,$$

with the Fermi level ξ_i defined by

$$\Delta\xi = \xi - \xi_i = k_B T \ln\left[\frac{2}{1+e^{-eV/k_B T}} \right]$$

and the parameter χ, which has to be determined self-consistently,

$$\chi = \hat{g}\frac{e}{cQ^{e,t}} \left[(1-\hat{c}) + \frac{c}{2} \int dE\, N_i f_i e^{(E-\xi_i)/k_B T} \right] .$$

The solution for χ then is

$$\chi = \hat{g}\frac{e}{cQ^{e,t}} \frac{2-\hat{c}}{2+\hat{g}}$$

and hence the electronic charge $Q^{e,t}$ can be determined. The expression for the hole charge coincides with the result in Sec. III,

$$Q^h = \frac{\lambda}{1+\lambda} e N_h, \quad \lambda = g j \tau_r \frac{c_h}{e} \frac{2-\hat{c}}{2+\hat{g}} \,,$$

for the case of a finite density N_h.

APPENDIX B

The small signal response of the junction for the model with a *continuous interface DOS* is determined for the case

where the interface is in thermal equilibrium (*relaxed interface*). The calculation proceeds along the same lines as in Sec. IV above.

The currents trapped and emitted by the interface acceptor states are[13]

$$j_t^e = j(1+e^{-eV/k_BT})[\hat{c}_0 - cN_\xi(e\tilde{\Phi}_b+\tilde{\xi}_i)e^{i\omega t}]$$

and

$$j_{em}^e = 2j_0\kappa_0[\hat{c}_0+cN_\xi(e\tilde{\Phi}_b+\tilde{\xi}_i)e^{i\omega t}] ,$$

$$\kappa_0 = e^{-\Delta\xi_0/k_BT} = \frac{1+e^{-eV_0/k_BT}-\hat{g}_{0c}}{2+\hat{g}_0}, \quad N_\xi = N_i(\xi_i) .$$

In the calculation of the hole charge Q^h we need the response of the trapped current,

$$\tilde{j}_t^h = \hat{g}_0 j_0 \left[\frac{e}{k_BT}(1-\hat{c}_0)\tilde{\Phi}_b + cN_\xi \left[1+\frac{1-\hat{g}_{0c}}{2+\hat{g}_0} \right](e\tilde{\Phi}_b+\tilde{\xi}_i) + \frac{g_0'}{g_0}\frac{2-\hat{c}_0}{2+\hat{g}_0}(\tilde{V}-\tilde{\Phi}_b) \right] - \frac{\lambda_0}{\tau_{r0}}\tilde{Q}^h ,$$

and of the recombination current,

$$\tilde{j}_{rec}^h = \frac{1}{\tau_{r0}}\tilde{Q}^h + \hat{g}_0 j_0 \frac{cN_\xi}{cN-\hat{c}_0}\frac{2-\hat{c}_0}{2+\hat{g}_0}(e\tilde{\Phi}_b+\tilde{\xi}_i) ,$$

$$N = \int dE\, N_i(E), \quad \tilde{Q}^e = eN_\xi(e\tilde{\Phi}_b+\tilde{\xi}_i) ,$$

to find

$$\tilde{Q}^h = \frac{\hat{g}_0 j_0 \tau_{r0}}{1+\lambda_0+i\omega\tau_{r0}} \left[\frac{e}{k_BT}(1-\hat{c}_0)\tilde{\Phi}_b + \frac{g_0'}{g_0}\frac{2-\hat{c}_0}{2+\hat{g}_0}(\tilde{V}-\tilde{\Phi}_b) + cN_\xi \left[1+\frac{1-\hat{g}_0}{2+\hat{g}_0} - \frac{1}{cN-\hat{c}_0}\frac{2-\hat{c}_0}{2+\hat{g}_0} \right](e\tilde{\Phi}_b+\tilde{\xi}_i) \right] .$$

We then use the rate equation for the total interface charge Q_i to determine first

$$e\tilde{\Phi}_b+\tilde{\xi}_i = \frac{e\hat{c}_0}{2ck_BTN_\xi}\frac{(1+\vartheta_r-\hat{g}_{0cr})\tilde{\Phi}_b - \left[\vartheta_r+\frac{1}{1+e^{eV_0/k_BT}}\right]\tilde{V}}{1+i\omega\tau_i+\mu_e} ,$$

$$\mu_e = \frac{\hat{g}_{0r}}{2\hat{c}_0}[2\hat{c}_0-1-(\lambda_0+i\omega\tau_{r0})v] ,$$

$$v = \frac{cN-2\hat{c}_0}{cN-\hat{c}_0}\frac{2-\hat{c}_0}{2+\hat{g}_0} ,$$

and using this result we find

$$\tilde{Q}_i = C_i^{\Phi,e}(\omega)\tilde{\Phi}_b - C_i^{V,e}(\omega)\tilde{V} ,$$

with

$$C_i^{\Phi,e}(\omega) = C_i^{e,e}(\omega)\left\{ 1+\lambda_0\hat{g}_{0cr}-\hat{g}_{0c} - \frac{\tau_{r0}}{\tau_i'}\frac{\hat{g}_{0r}}{\hat{c}_0}[1+(1-\hat{g}_{0c})v] + \vartheta_r\left[1+\frac{\tau_{r0}}{\tau_i}\left[1-\frac{\hat{g}_0}{2\hat{c}_0}v\right]+i\omega\tau_{r0}\right]\right\} ,$$

$$C_i^{V,e}(\omega) = C_i^{e,e}(\omega)\left\{ \frac{1}{1+e^{eV_0/k_BT}} + \vartheta_r\left[1+\frac{\tau_{r0}}{\tau_i}\left[1-\frac{\hat{g}_0}{2\hat{c}_0}v\right]+i\omega\tau_{r0}\right]\right\} ,$$

and

$$C_i^{e,e}(\omega) = \frac{e^2\hat{c}_0}{2ck_BT}\frac{1}{1+\mu^e+i\omega\tau_i}, \quad \tau_i' = 2\tau_i .$$

All the results for the injected current and for the admittance σ can be easily adapted to the present case by merely substituting the expressions above for the corresponding quantities in Sec. IV. In $\sigma_i(\omega)$ the term μ/f_{i0} is then changed to $2\mu^e$ [$f_{i0}\to f_{i0}(\xi_{i0})=\frac{1}{2}$].

The comparison of the present results with those of Sec. IV reveals only minor differences and the discussion of the negative capacitance applies equally well to the present case.

APPENDIX C

We outline the calculation for the small-signal admittance σ, taking the model with a *continuous interface DOS* where the electrons are *localized* within the interface. The steady-state properties of this model have been discussed in Appendix A. The two rate equations for the electrons (A1) and for the holes (A2) each possess a different recombination current j_{rec}^e and j_{rec}^h, and this renders the calculation more difficult than in the previous case.

In the calculation of the hole current $j^h = g(j_r^e - j_{rt}^{e,t} + j_{em}^{e,t}/2)$ we have to insert the expansions for the total trapping and emission currents,

$$\tilde{j}^h=\hat{g}_0 j_0\left[\frac{e}{k_BT}(1-\hat{c}_0)\tilde{\Phi}_b+\frac{c}{2e}(1-\chi_0)\tilde{Q}^{e,t}+\frac{\tilde{C}}{2}+\frac{g_0'}{g_0}\frac{2-\hat{c}_0}{2+\hat{g}_0}(\tilde{V}-\tilde{\Phi}_b)\right],$$

with

$$\tilde{Q}^{e,t}=e\int dE\,N_i(E)\tilde{f}_i,\quad \tilde{C}=c\int dE\,N_i(E)\frac{1}{f_{i0}(E)}\tilde{f}_i\,.$$

The expression for the modulation of the hole charge Q^h is

$$\tilde{Q}^h=\frac{\hat{g}_0 j_0\tau_{r0}}{1+\lambda_0+i\omega\tau_{r0}}\left[\frac{e}{k_BT}(1-\hat{c}_0)\tilde{\Phi}_b+\frac{g_0'}{g_0}\frac{2-\hat{c}_0}{2+\hat{g}_0}(\tilde{V}-\tilde{\Phi}_b)+\frac{c}{2e}\left[1-\frac{2+\hat{g}_0}{\hat{g}_0}\chi_0\right]\tilde{Q}^{e,t}+\frac{\tilde{C}}{2}\right].$$

We then determine the dynamics of a single-electron level at energy E by expansion of the electronic rate equation:

$$\left[i\omega eN_i+j_0cN_i(1+e^{-eV_0/k_BT})\frac{1}{f_{i0}}\right]\tilde{f}_i=j_0\frac{e}{k_BT}cN_i(1-f_{i0})[(1+e^{-eV_0/k_BT})\tilde{\Phi}_b-e^{-eV_0/k_BT}\tilde{V}]-\hat{g}_{0r}j_0\frac{Q_0^e}{Q_0^{e,t}}\left[\frac{e}{k_BT}(1-\hat{c}_0)\tilde{\Phi}_b+\frac{g_0'}{g_0}\frac{2-\hat{c}_0}{2+\hat{g}_0}(\tilde{V}-\tilde{\Phi}_b)+\frac{\tilde{C}}{2}+\frac{c}{2e}\left[1-\frac{2+\hat{g}_0}{\hat{g}_0}\chi_0\right]\tilde{Q}^{e,t}\right]. \tag{C1}$$

This supplies us, on the one hand, with an expression for the electronic charge modulation,

$$\tilde{Q}^e=\frac{N_if_{i0}(1-f_{i0})}{1+i\omega\tau_i'f_{i0}}\frac{e^2}{k_BT}\left[\tilde{\Phi}_b-\frac{\tilde{V}}{1+e^{eV_0/k_BT}}\right]-\frac{N_if_{i0}^2}{1+i\omega\tau_i'f_{i0}}\left[\hat{g}_{0cr}\frac{e^2\hat{c}_0}{ck_BT}\frac{e}{Q_0^{e,t}}\tilde{\Phi}_b+e\chi_{0r}'(\tilde{V}-\tilde{\Phi}_b)\right]-\frac{N_if_{i0}^2}{1+i\omega\tau_i'f_{i0}}\hat{g}_{0r}\frac{e}{2}\frac{e}{Q_0^{e,t}}\left[\frac{\tilde{C}}{c}+\left[1-\frac{e}{c}\frac{2-\hat{c}_0}{Q_0^{e,t}}\right]\frac{\tilde{Q}^{e,t}}{e}\right],$$

with

$$\chi_{0r}'=\hat{g}_{0r}'\frac{e}{cQ_0^{e,t}}\frac{2-\hat{c}_0}{2+\hat{g}_0},\quad \tau_i'=\frac{e}{j_0c}\frac{1}{1+e^{-eV_0/k_BT}}\,. \tag{C2}$$

Integration of (C1) over energy, on the other hand, leads to an equation for $\tilde{C}$,

$$\tilde{C}=\frac{1}{1+\hat{g}_{0r}/2}\left\{\frac{e\hat{c}_0}{k_BT}\left[(1-\hat{g}_{0cr})\tilde{\Phi}_b-\frac{\tilde{V}}{1+e^{eV_0/k_BT}}\right]-\hat{g}_{0r}'\frac{2-\hat{c}_0}{2+\hat{g}_0}(\tilde{V}-\tilde{\Phi}_b)-\frac{c}{e}\left[\frac{\hat{g}_{0r}}{2}\left[1-\frac{e}{c}\frac{2-\hat{c}_0}{Q_0^{e,t}}\right]+i\omega\tau_i'\right]\tilde{Q}^{e,t}\right\}. \tag{C3}$$

The integration over energy of Eq. (C2) is more difficult to perform. We have to determine the integral

$$\frac{e^2}{k_BT}\int dE\frac{N_if_{i0}(1-f_{i0})}{1+i\omega\tau_i'f_{i0}}\cong C^{e,l}(\omega)+\frac{e^2}{k_BT}\chi_0A\,, \tag{C4}$$

with

$$C^{e,l}(\omega)=e^2N_\xi\frac{\ln\left[1+\frac{i\omega\tau_i'}{1+\chi_0}\right]}{i\omega\tau_i'}\,,$$

and

$$A=\int dE\frac{N_if_{i0}^2}{1+\omega\tau_i'f_{i0}}\cong-\frac{k_BT}{e^2}C^{e,l}(\omega)-\chi_0A+\frac{Q_0^{e,t}}{e}-i\omega\tau_i'A\,.$$

From the last equation we find for A

$$A=\frac{Q_0^{e,t}}{e}\frac{1-(k_BT/e)(1/Q_0^{e,t})C^{e,l}(\omega)}{1+\chi_0+i\omega\tau_{r0}}\equiv\frac{Q_0^{e,t}}{e}\mathscr{A}\,. \tag{C5}$$

Equations (C4) and (C5) allow us now to perform the integration of (C2) and after elimination of $\tilde{C}$ with the help of (C3) we find for the electronic charge modulation

$$\tilde{Q}^{e,t}=\frac{1}{1+\beta^*}\left[C^{e,l}(\omega)\left[\tilde{\Phi}_b-\frac{\tilde{V}}{1+e^{eV_0/k_BT}}\right]+\frac{2e\chi_0 A}{2+\hat{g}_{0r}}\left[\frac{e}{k_BT}\frac{\lambda_0+i\omega\tau_{r0}}{1+\lambda_0+i\omega\tau_{r0}}\tilde{\Phi}_b-\frac{g'_{0r}}{g_0}(\tilde{V}-\tilde{\Phi}_b)\right]\right],$$

with

$$\beta^*=\frac{\hat{g}_{0r}}{2+\hat{g}_{0r}}\mathscr{A}\left[1-\frac{e}{c}\frac{2-\hat{c}_0}{Q_0^{e,t}}-i\omega\tau_i'\right].$$

The result for the total charge dynamics finally is

$$\tilde{Q}_i=C_i^{\Phi,l}(\omega)\tilde{\Phi}_b-C_i^{V,l}(\omega)\tilde{V},$$

with

$$C_i^{\Phi,l}(\omega)=C_i^{e,l}(\omega)+\frac{\hat{g}_{0r}}{2+\hat{g}_{0r}}\frac{e^2(2-\hat{c}_0)}{ck_BT}\mathscr{A}\left[\frac{\lambda_0+i\omega\tau_{r0}}{1+\hat{g}_0/2}\frac{1-\beta^0}{1+\beta^*}-\frac{\beta^0}{\beta^*}\right]+\frac{\chi'_{0r}Q_0^{e,t}}{1+\hat{g}_{0r}/2}\mathscr{A}\frac{1+\beta^0/\beta^*}{1+\beta^*},$$

$$C_i^{V,l}(\omega)=C_i^{e,l}(\omega)\frac{1}{1+e^{eV_0/k_BT}}+\frac{\chi'_{0r}Q_0^{e,t}}{1+\hat{g}_{0r}/2}\mathscr{A}\frac{1+\beta^0/\beta^*}{1+\beta^*},$$

$$\beta^0=\beta^*\frac{\tau_{r0}}{\tau_i'}\frac{1}{\mathscr{A}}.$$

The calculation of the current injected into the neighboring grain is a rather tedious but straightforward task. By a clever arrangement of terms, the expression simplifies considerably, such that we can put the final result for the admittance into a reasonable form:

$$\sigma^l=[(1-\vartheta_r^l-e^{-eV_0/k_BT})\sigma_0^l+\sigma_i^l(\omega)+i\omega C_l]\frac{C_r+C_i^{V,l}(\omega)}{C_r+C_l+C_i^{\Phi,l}(\omega)}+\left[(\vartheta_r^l+e^{-eV_0/k_BT})\sigma_0^l-\frac{1}{1+e^{eV_0/k_BT}}\sigma_i^l(\omega)\right],$$

with the modified zero-bias dc conductance

$$\sigma_0^l=j_0\frac{e}{k_BT}\left[1-\frac{\hat{c}_0}{2}\right]\left[1+\frac{\hat{g}_0}{2+\hat{g}_0}\right],$$

and the correction by the interface dynamics

$$\sigma_i^l(\omega)=j_0\frac{c}{2e}C_i^{e,l}(\omega)\frac{1}{1+\beta^*}\times\left[(1+i\omega\tau_i')-e^{-eV_0/k_BT}(1-i\omega\tau_i')+\frac{\hat{g}_{0r}}{2+\hat{g}_{0r}}(1-i\omega\tau_i')\right].$$

The dependence of the yield g on the barrier parameter Φ_b+V introduces the term

$$\vartheta_r^l=\frac{\hat{g}'_{0r}}{2+\hat{g}_{0r}}\frac{1}{1+\hat{g}_0}\left[\frac{k_BT}{e}\right]^2\frac{C_i^{e,l}(\omega)}{Q_0^{e,t}}.$$

The results for the model treating the interface states as localized states, which exchange their particles only with the bulk, are very cumbersome. The complication of different recombination currents $j_{\rm rec}^e$ and $j_{\rm rec}^h$ (note that $j_{\rm rec}^{e,t}=j_{\rm rec}^h$) renders the calculations far more difficult than in the other cases. A numerical check shows, however, that the above results differ only slightly from those of the equilibrated interface (see also the discussion in BG). Note that the interface capacitance $C_i^{\Phi,l}(\omega)$ contains a negative term similar to the other models,

$$C_i^{\Phi,l}(\omega)\cong C_i^{e,l}(\omega)-\hat{g}_{0r}\frac{e^2}{ck_BT}\frac{\tau_{r0}}{\tau_i'}+\hat{g}_{0r}\frac{e^2}{ck_BT}\mathscr{A}\left[\lambda_0+i\omega\tau_{r0}+\frac{g'_0}{g_0}\left[1+\frac{1}{\mathscr{A}}\frac{\tau_{r0}}{\tau_0'}\right]\right].$$

[1]For a recent review, see *Polycrystalline Semiconductors*, Vol. 57 of *Springer Series in Solid-State Sciences*, edited by G. Harbeke (Springer, Berlin, 1985).

[2]A. Bourret, in *Polycrystalline Semiconductors*, Ref. 1.

[3]R. E. Thomson and D. J. Chadi, Phys. Rev. B **29**, 889 (1984); H. J. Möller and H. H. Singer, in *Polycrystalline Semiconductors*, Ref. 1; D. P. DiVincenzo, O. L. Alerhand, M. Schlüter, and J. W. Wilkins, Phys. Rev. Lett. **56**, 1925 (1986).

[4]J. Bernasconi, H. P. Klein, B. Knecht, and S. Strässler, J. Electron. Mater. **5**, 473 (1976); Solid State Commun. **21**, 867 (1977).

[5]L. M. Levinson and H. R. Philipp, J. Appl. Phys. **47**, 1117 (1976); **49**, 6142 (1978); G. D. Mahan, L. M. Levinson, and H. R. Philipp, J. Appl. Phys. **50**, 2799 (1979).

[6]G. E. Pike and C. H. Seager, J. Appl. Phys. **50**, 3414 (1979).

[7]C. H. Seager and G. E. Pike, Appl. Phys. Lett. **37**, 747 (1980); **40**, 471 (1982).

[8]M. G. Spencer, W. J. Schaff, and D. K. Wagner, J. Appl. Phys.

54, 1429 (1983).

[9]G. C. McCognial, D. J. Thomson, J. G. Shaw, and H. C. Card, Phys. Rev. B **28**, 5098 (1983).

[10]H. F. Mataré, J. Appl. Phys. **56**, 2605 (1984); C. R. M. Grovenor, J. Phys. C **18**, 4079 (1985).

[11]J. Werner and H. Strunk, J. Phys. C **1**, 89 (1982); J. Werner, Ph.D. thesis, University of Stuttgart, 1983; and in *Polycrystalline Semiconductors,* Ref. 1.

[12]G. E. Pike, Phys. Rev. B **30**, 795 (1984).

[13]G. Blatter and F. Greuter, in *Polycrystalline Semiconductors,* Ref. 1.

[14]G. Blatter and F. Greuter, Phys. Rev. B **33**, 3952 (1986).

[15]G. E. Pike, in *Grain Boundaries in Semiconductors,* edited by H. J. Leamy *et al.* (North-Holland, Amsterdam, 1982), p. 369.

[16]G. E. Pike, P. L. Gourley, and S. R. Kurtz, Appl. Phys. Lett. **43**, 939 (1983).

[17](a) F. Greuter, J. Bernasconi, and R. S. Perkins, Am. Ceram. Soc. Bull. **63**, 480 (1984); and unpublished. (b) G. E. Pike, S. R. Kurtz, P. L. Gourley, H. R. Philipp, and L. M. Levinson, J. Appl. Phys. **57**, 5512 (1985); Am. Ceram. Soc. Bull. **63**, 480 (1984); G. E. Pike, C. H. Seager, and R. G. Dosch, in *Microscopic Identification of Electronic Defects in Semiconductors,* Materials Research Society Symposia Proceedings, edited by W. M. Johnson, S. G. Bishop, and G. D. Watkins (North-Holland, Amsterdam, 1985), Vol. 46, p. 409.

[18]F. Greuter and E. Gisler, Europhys. Conf. Abstr. **9C**, 302 (1985); and unpublished.

[19](a) R. K. Mueller, J. Appl. Phys. **32**, 635 (1961). The result applies to a thermionic emission model for the electron transport but a diffusion limited approach leads to a similar result. (b) G. E. Pike, Phys. Rev. B **30**, 3274 (1984).

[20]L. H. Holway, Jr., Phys. Rev. Lett. **28**, 280 (1972); L. H. Holway, Jr., and D. W. Fradin, J. Appl. Phys. **46**, 279 (1975).

[21]H. Fröhlich and N. F. Mott, Proc. R. Soc. London, Ser. A **171**, 496 (1939); H. Fröhlich, *ibid.* **160**, 230 (1937); Adv. Phys. **3**, 325 (1954).

[22]Masamichi Tsuboi, J. Chem. Phys. **40**, 1326 (1964).

[23]R. P. Feynman, *Statistical Mechanics* (Benjamin, Massachusetts, 1972), p. 223.

[24]*Landolt-Börnstein,* edited by O. Madelung (Springer, Berlin, 1982), Vol. 176, and references therein.

[25]G. Baym, *Lectures on Quantum Mechanics* (Benjamin, Masschusetts, 1973), p. 213.

[26]E. Conwell and V. F. Weisskopf, Phys. Rev. **77**, 388 (1950).

[27]E. O. Kane, Phys. Rev. **159**, 624 (1967).

[28]J. Geist and W. K. Gladden, Phys. Rev. B **27**, 4833 (1983).

[29]R. C. Alig, S. Bloom, and C. W. Struck, Phys. Rev. B **22**, 5565 (1980).

[30]M. V. Fischetti, D. J. DiMaria, S. D. Brorson, T. N. Theis, and J. R. Kirtley, Phys. Rev. B **31**, 8124 (1985).

[31]U. Baranger and J. W. Wilkins, Phys. Rev. B **30**, 7349 (1984).

[32]C. Jacoboni and L. Reggiani, Rev. Mod. Phys. **55**, 645 (1983).

[33]P. Hesto, Surf. Sci. **132**, 623 (1983).

[34]G. D. Mahan, J. Appl. Phys. **58**, 2242 (1985).

[35]S. A. Trugman and A. J. Taylor, Phys. Rev. B **33**, 5575 (1986).

[36]P. A. Wolff, Phys. Rev. **95**, 1415 (1954).

[37]W. Shockley, Solid-State Electron. **2**, 35 (1961).

[38]G. A. Baraff, Phys. Rev. **128**, 2507 (1962).

[39]M. Sparks, D. L. Mills, R. Warren, T. Holstein A. A. Maradudin, L. J. Sham, E. Loh, Jr., and D. F. King, Phys. Rev. B **24**, 3519 (1981).

[40]B. K. Ridley, J. Phys. C **16**, 3373 (1983).

[41]M. G. Burt, J. Phys. C **18**, L477 (1985).

[42]W. P. Dumke, Phys. Rev. **167**, 783 (1968).

[43]G. E. Uhlenbeck and L. S. Ornstein, Phys. Rev. **36**, 823 (1930). This work treats the distribution function in energy space for a *time*-dependent problem.

[44]A. Kobayashi, O. F. Sankey, S. M. Volz, and J. D. Dow, Phys. Rev. B **28**, 935 (1983).

[45]H. Hartmann, R. Mach, and B. Selle, *Current Topics in Material Science,* edited by E. Kaldis (North-Holland, Amsterdam, 1982), Vol. 9.

[46]R. H. Bube, *Photoconductivity of Solids* (Wiley, New York, 1960).

[47]For practical calculations the denominator $2+\hat{g}$ in λ is substituted by 2 ($\hat{g} \ll 1$).

[48]As a further stabilization mechanism the band-band recombination within the depletion region has been considered, however with no convincing success.

[49]A time-dependent quantity $u(t)$ is approximated to first order by $u_0+\tilde{u}\exp(i\omega t)$. Only the expansion of Φ_b is defined with a minus sign, $\Phi_b(t)=\Phi_{b0}-\tilde{\Phi}_b\exp(i\omega t)$.

[50]The "decoration" of g is straightforward: $g_0=g(V_0+\Phi_{b0})$, $g_{0c}=g_0(1-\hat{c}_0)/\hat{c}_0$, $\hat{g}_0=g_0\hat{c}_{h0}$, $\hat{g}_{0c}=\hat{g}_0(1-\hat{c}_0)/\hat{c}_0$.

[51]If the electronic DOS at the interface is not bounded from above (e.g., a broad rectangular DOS) the capacitance remains at its large value. With increasing bias the hole dynamics become dominant, however, and the capacitance turns abruptly to negative values. The filling of the electron DOS is therefore not a prerequisite for a negative capacitance.

[52]M. Rossinelli, G. Blatter, and F. Greuter, in *British Ceramic Proceedings,* edited by B. C. H. Steele (Institute of Ceramics, Shelton, U.K., 1985), Vol. 36, pp. 1–17.

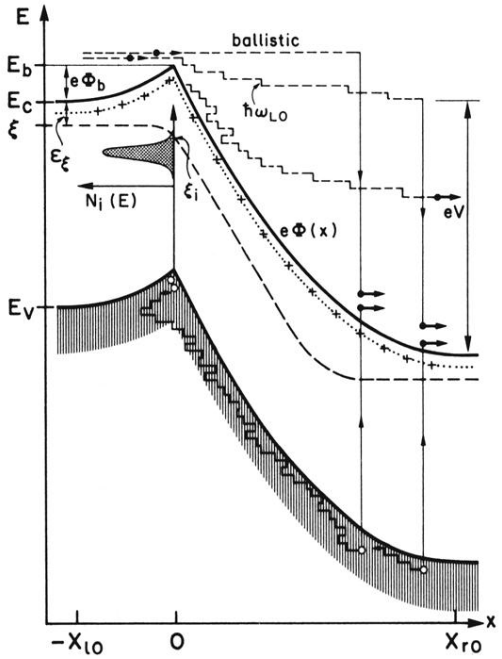

FIG. 1. Energy-band diagram for a double Schottky barrier at a grain boundary under large applied bias V. The mechanisms of hot-electron transport and pair creation are sketched.